Optical Materials 131 (2022) 112695

Contents lists available at ScienceDirect

Optical Materials

journal homepage: www.elsevier.com/locate/optmat

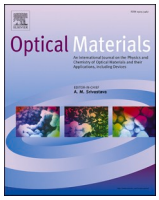

Research Article

Functionalization of TiO_2 inverse opal structure with atomic layer deposition grown Cu for photocatalytic and antibacterial applications

Khai Pham [a,*], Harri Ali-Löytty [b,**], Jesse Saari [b], Muhammad Zubair [b], Mika Valden [b], Kimmo Lahtonen [c], Niko Kinnunen [a], Marianne Gunell [d,e], Jarkko J. Saarinen [a]

[a] Department of Chemistry, University of Eastern Finland, Joensuu, FI-80101, Finland
[b] Surface Science Group, Photonics Laboratory, Tampere University, P.O. Box 692, FI-33014, Tampere University, Finland
[c] Faculty of Engineering and Natural Sciences, Tampere University, P.O. Box 692, FI-33014, Tampere University, Finland
[d] Department of Clinical Microbiology, Turku University Hospital, 20521, Turku, Finland
[e] Department of Medical Microbiology and Immunology, University of Turku, 20500, Turku, Finland

ARTICLE INFO

Keywords:
Inverse opal
Atomic layer deposition (ALD)
TiO_2
Cu
Photocatalytic activity
CO_2 reduction
Antimicrobial activity

ABSTRACT

TiO_2 inverse opal (IO) structure surfaces were functionalized with a sub-monolayer amount of Cu by atomic layer deposition (ALD) and tested for photocatalytic and antimicrobial applications. Decomposition of acetylene (C_2H_2) into CO_2 and reduction of CO_2 into CH_4 were tested in the gas phase and photodegradation of methylene blue (MB) was tested in the liquid phase. Antimicrobial activity was tested against Gram-positive *Staphylococcus aureus* (*S. aureus*) bacteria. ALD Cu without any post-deposition heat treatment (HT) decreased the photo degradation rate of both C_2H_2 and MB but improved the activity towards CO_2 reduction. ALD Cu increased MB photodegradation rate and antimicrobial activity only after HT at 550 °C, which was linked to the improved chemical stability Cu after the HT. The same HT decreased the activity towards CO_2 reduction and decomposition of C_2H_2. The HT induced desorption of loosely bound ALD $Cu^{+/2+}$ from the TiO_2 IO surface and the remaining $Cu^{+/2+}$ was reduced to Cu^+. The photocatalytic and antimicrobial activity of TiO_2 IO can be tailored by the addition of a sub-monolayer amounts of Cu with performance depending on the targeted reaction.

1. Introduction

New innovations in materials science are continuously sought to tackle the grand challenges in society including renewable fuel production, mitigation of CO_2 emissions, and most acutely, fight against the pandemia. Functionalization of photocatalyst materials is a promising strategy to response to these kinds of challenges. Recently, TiO_2 inverse opal (IO) structures have received large interest due to high surface area, unique optical characteristics, and various applications ranging from decomposition pollutants [1] to solar fuel production [2]. Functionalization of TiO_2 surface with transition metals or their oxides can increase the activity by increasing the visible light absorption, facilitating the photoinduced charge separation or catalyzing targeted chemical reactions. Successful functionalization requires optimization of transition metal loading and often involve post-deposition thermal treatments. Atomic layer deposition allows for controlled coating of porous structures and has been earlier applied to functionalize IO structures with transition metal oxides (Al_2O_3, SiO_2, and TiO_2) for photocatalytic applications [3].

Combination of TiO_2 and Cu has a great potential for environmental purification and solar-energy conversion since both materials are nontoxic and resistant to photo-corrosion with abundant availability [4]. Cu_xO-TiO_2 nanocomposites have been fabricated by various physical and chemical methods including ball milling [4], sol-gel [5], chemical vapor deposition (CVD) [6], and atomic layer deposition (ALD) [7]. Recently, the addition of single-atom Cu on TiO_2 photocatalyst has been reported to boost the activity of material to 66 times in the reduction of CO_2 reactions. However, traditional methods of deposited often produced non-uniformly distributed of the atom on the surface of photocatalyst [8,9]. The self-limiting nature of the ALD cycles allows sub-monolayer thickness control of the deposited films with high repeatability and surface uniformity. Moreover, ALD allows conformal coating of large aspect (length-to-diameter) ratio objects with a uniform film. Therefore, ALD is a widely used technique especially in

* Corresponding author.
** Corresponding author.
E-mail addresses: khai.pham@uef.fi (K. Pham), harri.ali-loytty@tuni.fi (H. Ali-Löytty).

https://doi.org/10.1016/j.optmat.2022.112695
Received 6 May 2022; Received in revised form 20 June 2022; Accepted 3 July 2022
Available online 10 July 2022

semiconductor industry but is also used as an advanced tool for nanotechnology research.

Motivated by single-atom catalysts concept, in this work TiO_2 IO framework was functionalized using ALD Cu coating for selected catalytic reactions. Photocatalytic activity of the samples under the ultraviolet A (UVA) excitation was assessed in the gas phase by the decomposition of acetylene (C_2H_2) into CO_2 and reduction of CO_2 into CH_4, and in the liquid phase by the degradation of methylene blue (MB). Antimicrobial activity was tested against Gram-positive *Staphylococcus aureus* (*S. aureus*) bacteria. The improved photocatalytic activity of the Cu ALD coated TiO_2 IO materials is discussed in terms of interfacial chemistry and charge-transfer in the formed heterostructure.

2. Materials and methods

2.1. TiO_2 inverse opal structure preparation

TiO_2 IO structure was synthesized using polystyrene spheres with a diameter of 400 nm (PS400) as a template. Transparent, homogenous solution of 5 ml titanium (IV) isopropoxide (TTIP, 97%, Sigma-Aldrich), 47 ml of ethanol (99.5%, Etax AA), 2 ml of hydrochloric acid (37%, VWR chemicals) and 2 ml of deionized (DI) water were used as a precursor.

PS400 was prepared by a free-radical emulsion polymerization from styrene (99%, Acros Organics), sodium dodecyl sulfate (SDS, 98.5%, Sigma-Aldrich) and ammonium persulfate (APS, 98%, Sigma-Aldrich). First, the seed solution of 200 nm PS spheres was prepared by mixing 200 mg of SDS and 160 ml of DI water in a flask and heated to 70 °C while stirred at 500 rpm under nitrogen flow. 20 g of styrene was poured into this solution and stirred for 0.5 h that was followed by dropwise addition of 20 ml of APS solution (200 mg of APS in 20 ml of DI water) into the reactor. The system was kept at that condition for 20 h and the seed solution of 200 nm PS spheres was obtained. Next, 30.4 ml of 200 nm seed solution and 25 mg of SDS were diluted with 150 ml deionized water and heated to 70 °C under nitrogen flow to make PS400. After stabilizing at 70 °C, 20 ml solution of APS (28 mg APS in 20 ml DI water) was added. As a final step, 21.6 g styrene was slowly added to the reactor solution, and the reaction was again maintained for 20 h to get PS400 solution.

PS400 template was loaded on soda-lime microscope glass (Thermo Scientific) by sonicating 0.6 ml of PS400 in 25 ml deionized water for 0.5 h. Two glass microscope slides were first washed in distilled water, immersed vertically into PS400 solution, and left at 65 °C for 2 days for vaporization. These PS coated glass substrate was then heated up 80 °C for 2 h to improve both quality and durability of the generated opal structure. Finally, the opal template was dipped into TiO_2 precursor solution two times to ensure void filling of the opal template. The sample was kept in ambient conditions overnight. The sample was then calcinated at 550 °C for 5 h with a ramp rate of 2 °C/min.

2.2. ALD deposition of Cu

ALD deposition of Cu was carried out using a Picosun Sunale ALD R200 Advanced reactor. Copper(II)-bis-(dimethylamino-2-propoxide) ($Cu(dmap)_2$, min. 97%, STREM Chemicals, Inc.), Milli-Q® type 1 ultrapure water, and Ar (99.9999%, Oy AGA Ab, Finland) were used as the Cu precursor, O precursor, and carrier/purge/venting gas, respectively. During the deposition $Cu(dmap)_2$ precursor source was held at 100 °C to maintain a sufficient vapor pressure, the water source was kept at 18 °C by a Peltier element for stability control, and the growth chamber was kept at 150 °C. The continuous Ar flow in the $Cu(dmap)_2$ and H_2O lines was 100 sccm. The ALD Cu cycle consisted of the 0.7 s $Cu(dmap)_2$ pulse followed by the 30.0 s purge period to pump the excess precursor and the reaction by-products from the reaction chamber before introducing H_2O. Analogously, the pulse and the purge times for H_2O pulse were 0.3 s and 6.0 s, respectively. Two sets of TiO_2 IO samples were prepared with 10 and 150 ALD Cu cycles. The growth rates of 0.045–0.090 Å/cycle have been reported for the ALD process depending on the water dosage [10].

2.3. Sample characterization

The morphological information of the prepared surfaces was acquired using field-emission scanning electron microscope (FE-SEM, Hitachi S-4800). UV/Vis/NIR spectrometer (PerkinElmer Lambda 900) was used to measure the absorption spectra of the samples. The crystalline properties of the prepared materials were characterized using X-ray diffraction (XRD, Bruker-AXSD8 Advance) with Cu Kα as the radiation source. The diffraction patterns were measured from 10° to 90° at 2θ scale with a step size of 0.05°/min.

The X-ray photoelectron spectroscopy (XPS) measurements were carried out in an ultrahigh vacuum (UHV) system with base pressure below 1×10^{-8} mbar. XPS was measured using non-monochromatized Al Ka X-rays ($h\nu = 1486.6$ eV) generated by a twin anode X-ray source (8025 Twin anode X-Ray source, V. G. Microtech) and a hemispherical electron spectrometer (CLAM4 MCD LNo5, V. G. Microtech). The element chemical state was determined from the XPS spectra by least-square fitting of asymmetric Gaussian–Lorentzian line shapes after subtracting a Shirley type background. The analysis was conducted using CasaXPS software version 2.3.17PR1.1 [11] with the Scofield photoionization cross-sections as relative sensitivity factors [12]. The binding energy scale for core level XPS was calibrated according to Ti^{4+} $2p_{3/2}$ that was set to 458.8 eV. The mean free path of Ti 2p photoelectrons in Cu (1.9 nm [13]) was used to approximate the ALD Cu overlayer thickness [14]. The upper approximation to the Cu loading here, based on the attenuation of photoelectron signal from the substrate by a homogeneous over layer, is 1.1 nm.

2.4. Photocatalytic activity assessment

Photodegradation of methylene blue (MB) on IO TiO_2 was measured in liquid phase using a test protocol described in Ref. [15], which was adapted from the standard (ISO 10678:2010). TiO_2 IO coated microcopy slides were placed in a quartz cuvette filled with 15 ml of 1.5 ppm methylene blue (MB) aqueous solution. The sample was first kept in dark for 60 min to allow MB adsorption onto the film surface. The photodegradation of MB was then initiated and conducted by UVA light irradiation (300–400 nm, optical power of 20 mW/cm^2) under convection induced by a magnetic stirrer. The film area exposed to the UVA light was 6.25 cm^2. MB concentration was measured online by monitoring transmission (T) of 635 nm laser beam through the cuvette.

Photocatalytic activity of the thin film coated TiO_2 IO structures was studied by decomposition of acetylene (C_2H_2) into carbon dioxide (CO_2) that was carried out using an in-house built gas-phase reactor at the UEF as reported earlier [3,6]. Two glass substrates were placed into the reactor chamber (20 cm^2 film area). The reactor was filled with a controlled mixture of technical air and acetylene. High intensity UVA light (XBO 450W OFR from Osram, light housing from Newport, USA) was used as a light source. Oxidation of C_2H_2 into CO_2 was monitored using an infrared CO_2 detector (Vaisala GMP343, FI) inside the reactor.

Photocatalytic CO_2 reduction tests in the gas-phase were performed using an in-house-built recirculating batch reactor comprising of a quartz photoreactor (250 ml photoelectrochemical cell, Pine Research, NC, USA), peristaltic pump (Masterflex, Cole-Parmer, IL, USA), gas chromatography unit with two gas sampling valves (Thermo scientific TRACE 1310, MA, USA), a flow meter (G Series, Swagelok, OH, USA), a pressure gauge (Baratron®, MKS Instruments, MA, USA), gas inlets and a vacuum pump (SH-110 Dry Scroll Vacuum Pump, Agilent Technologies, CA, USA). Before sealing the reactor, 10 ml ultrapure water (18.2 MΩ cm, Merck Milli-Q®) was added to the bottom of the photoreactor and a microscopy slide with the photocatalyst coating was supported in upright position above the liquid. The reactor was then evacuated and filled with CO_2 (99.99% CO_2, Aga, Finland) in three repetitive cycles to

remove all impurities from the system. The photoreactor was finally filled with 760 torr CO_2 and kept it in dark for 30 min to guarantee the adsorption-desorption equilibrium. During the test, the gas was recirculated between the gas chromatography (GC) and the photoreactor with the peristaltic pump. The photocatalytic reaction was initiated by illuminating the photocatalyst (3.6 cm^2 film area) by UVA light (300–400 nm, optical power of 51 mW/cm^2) from the light source (MAX-350 equipped with UV–Vis mirror module and a 400 nm short pass filter XHS0400, Asahi Spectra Co., Ltd., Japan). After every 30 min, a gas-phase sample was injected to the GC via the two gas sampling valves (GSV) using N_2 as the carrier gas in the GC. GSVs were connected to a thermal conductivity detector (TCD) and a flame ionization detector (FID) via TG-Bond Msieve 5A and TG-BOND Q 5A columns (Thermo scientific TRACE 1310, MA, USA), respectively. The GC response was calibrated before each test using a gas mixture consisting of O_2, CO_2, H_2, CO, CH_4, C_2H_4 and C_2H_6 (0.5 vol.-% each) in N_2 (Linde plc, Ireland). Each test was performed for 2 h and the production rate was normalized to the illuminated surface area and time.

Antimicrobial tests were carried out using a touch test method [16] with Gram-positive (*Staphylococcus aureus* ATCC 29213 0.5 McF 50 μl) bacteria. In touch test procedure, bacteria culture was diluted in 0.9% NaCl to 0.5 McFarland standard i.e., approximately 1.5×10^8 colony--forming units (CFUs) in a milliliter (CFU/ml). The sample surface was exposed with 50 μl of bacterial suspension and incubated at a room temperature for 24 and 48 h in an empty Petri dish. After incubation, the sample surface was pressed against a blood agar plate for 30 s and then agar plates were incubated again at +37 °C. The number of CFUs was calculated from the agar plates after 24 h.

3. Results and discussion

3.1. Characterization of Cu–TiO_2 IO

TiO_2 IO structures were functionalized with Cu by ALD technique using 10 and 150 ALD cycles of Cu (<1.1 nm Cu loading). The TiO_2 IO reference and TiO_2 IO coated samples with 10 and 150 cycles of Cu are denoted as no Cu, 10 c Cu, and 150 c Cu, respectively. The effect of post ALD deposition heat treatment (HT) was studied using the same conditions (550 °C in air) with the TiO_2 IO calcination treatment. HT samples were named as 10 c Cu + HT and 150 c Cu + HT. The as-prepared samples were examined by SEM, XRD, UV–Vis, and XPS.

First, the TiO_2 IO samples before and after ALD Cu coating were characterized by SEM as shown in Fig. 1a and b. As can be seen clearly from Fig. 1a, all PS spheres were completely removed during calcination, and there were no traces of precursor left on the sample surface. IO structures were well connected in hexagonal close packed array and exhibited a face-centered cubic (FCC) plane (111) orientation. No cracks were observed at the magnification of x80k (a few micrometers scale). At a lower magnification of x300 (Fig. S1), cracks were observed in all samples at a few hundred micrometers scale. This is unavoidable due to the shrinkage of the PS spheres during the calcination process that was estimated to be around 30%.

The ALD deposition of Cu on the surface of TiO_2 IO had only little effect to the contrast of SEM images, even for the sample with 150 ALD cycles (Fig. 1b). The result suggests that the distribution of ALD Cu deposits is uniform and conformal, and that the Cu loadings are within the targeted range of few nanometers. We note that the nominal Cu loading is of the order of monolayers, and in the case of 10 c sample it is likely that Cu only partially covers the TiO_2 IO surface. The HT did not affect the contrast of SEM images. In particular, no Cu particles were detected on the surface (Fig. S2).

XPS was utilized to investigate the chemical composition of the Cu–TiO_2 IO nanocomposites. Table 1 shows atomic Cu/Ti ratios for the analyzed samples. The Cu/Ti ratio was found to increase and the Ti 2p intensity decreased with the increasing number of ALD Cu cycles. The Ti 2p signal intensity was attenuated to 57% for the 150 c sample

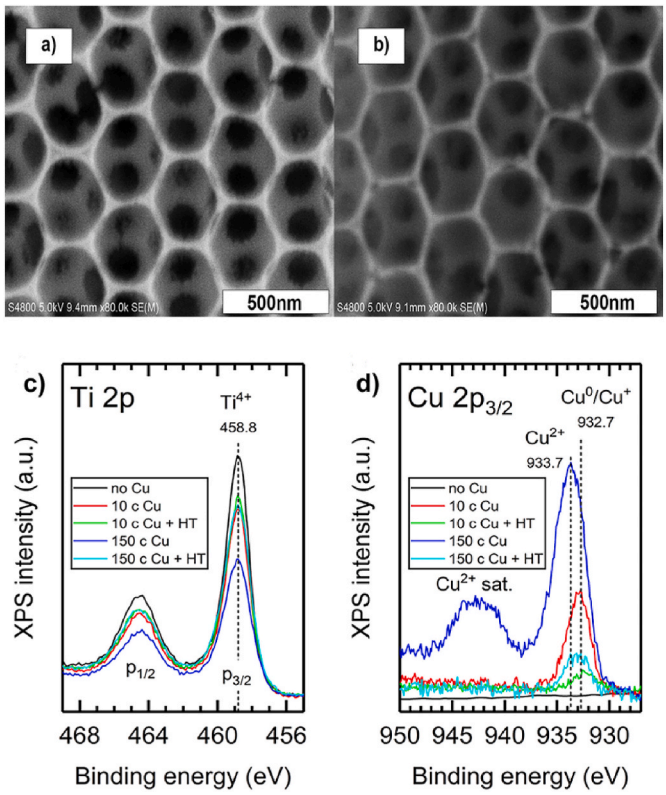

Fig. 1. SEM images of (a) no Cu and (b) 150 c Cu samples. XPS spectra of (c) Ti 2p and (d) Cu $2p_{3/2}$ transitions for different TiO_2 IO samples.

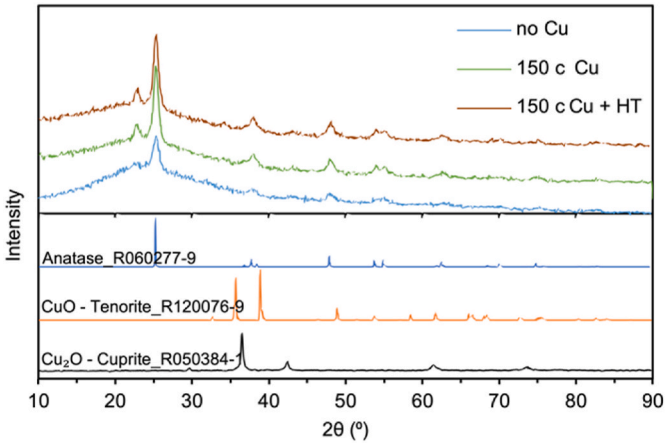

Fig. 2. XRD patterns of no Cu and 150 c Cu before and after HT. XRD reference patterns below are from RRUF database [17].

compared to the initial intensity measured for "no Cu" sample. Assuming XPS intensity attenuation by a homogeneous overlayer according to the Beer–Lambert law level this corresponds to 1.1 nm thick Cu film, which is in line with the nominal growth rate.

The XPS spectra of Ti 2p and Cu 2p species are shown in Fig. 1c and d. In Ti 2p spectra have two peaks at 458.8 eV and 464.6 eV corresponding to Ti $2p_{3/2}$ and Ti $2p_{1/2}$, respectively, and can be assigned to Ti^{4+} in anatase-TiO_2 [18]. Neither the ALD Cu process nor the HT induced any changes to the chemical state of Ti. Cu $2p_{3/2}$ spectra showed two clearly distinguishable peaks: one at 931–935 eV and another at 940–945 eV. The former is an elastic photoemission peak that can be convoluted to Cu^{2+} at 933.7 eV and indistinguishable Cu^0 or Cu $^+$ at 932.7 eV [19], albeit the presence of metallic Cu is considered unlikely under the

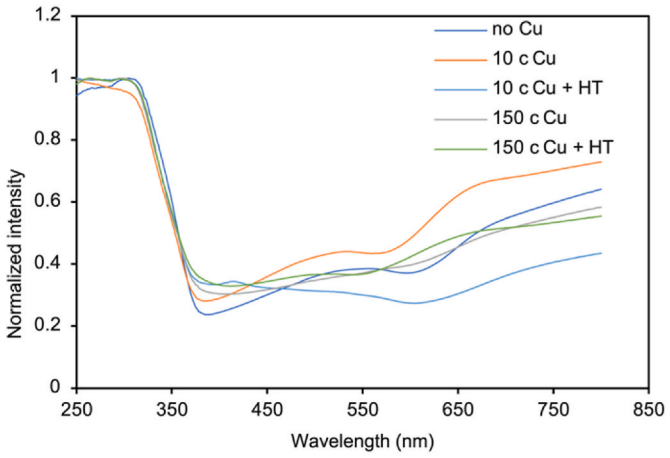

Fig. 3. UV–Vis absorption spectra of TiO_2 IO structure with 10 and 150 cycles of ALD Cu before and after heat treatment.

Table 1
Cu to Ti atomic ratios at the surface (XPS) and in the bulk (ICP-MS) of TiO_2 IO samples.

Atomic ratio	Cu/Ti surface	Cu/Ti bulk
no Cu	0.00	0.000
10 c Cu	0.13	0.006
10 c Cu + HT	0.03	0.007
150 c Cu	0.83	0.048
150 c Cu + HT	0.06	0.006

Table 2
Antimicrobial testing results using Gram-positive *S. aureus*.

Bacteria	Incubation time (h)	bare glass	no Cu	10 c Cu + HT	150 c Cu + HT
S. aureus	24	+++	+++	+++	+++
	48	++	++	+	++

+, ++ and +++ correspond to 10^3–10^4 CFU, 10^4–10^5 CFU and $>10^5$ CFU, respectively. – no growth.

studied conditions. The latter peak is a satellite peak characteristic to Cu^{2+} species. The chemical composition of Cu in ALD Cu samples was found different. The 150c Cu sample had primarily Cu^{2+} (CuO) whereas the 10c Cu sample had only Cu^{+} (Cu_2O). The differences may have resulted from the ALD process but here it is more likely that the observed difference was affected by the exposure to the air before XPS measurement. Thus, the chemical composition of ALD Cu was concluded to be $Cu_2^{+}O$ that oxidizes to $Cu^{2+}O$ in air with time. The growth of Cu_2O using the same ALD Cu process was reported earlier by Avila et al. [10].

The heat-treatment at 550 °C had two strong effects to the surface composition. Firstly, after the HT no Cu^{2+} satellite peak was detected, which indicates that the HT induced the reduction of Cu^{2+}. Ti forms more stable oxides than Cu, and therefore, any vacancies in the TiO_2 substrate could have mediated the Cu^{2+} reduction [20]. This contradicts with the oxidation of Cu foil that forms a $Cu^{2+}O$ surface oxide under the same conditions [21]. Secondly, upon the HT the Cu 2p intensities (Fig. 1d) decreased and Ti 2p intensities (Fig. 1c) increased resulting in a decrease in the atomic Cu/Ti ratio (Table 1). These changes could have been caused either by the diffusion of Cu into the TiO_2 substrate, by a change in the morphology of Cu from a thin film to clusters or by the desorption of Cu species from the surface. Studies showing thermally induced incorporation of Cu into the TiO_2 matrix either, at substitutional or interstitial site, are rare. Cu-doped TiO_2 has been prepared by sol-gel methods involving high-temperature calcination treatment, and Cu has been suggested to locate at an interstitial position in the TiO_2 matrix [22–24]. After calcination at 500 °C only Cu^{+} species were reported to exist at the surface by XPS [23,24]. On the other hand, Cu forms easily particles on TiO_2 surface and annealing is known to induce coarsening of Cu clusters already at temperatures as low as 300 °C [25]. Therefore, our interpretation is that the HT induced morphological changes to the Cu either clustering of Cu_2O on TiO_2 surface or diffusion of Cu^{+} into the TiO_2 matrix and also desorption of loosely bound Cu species. Analysis of bulk composition by ICP-MS (Table 1) revealed that after the HT the Cu concentration of 150 c sample had decreased to the same level with 10 c sample (0.6% Cu). Considering that no Cu particles were detected on surface by SEM these results together suggest diffusion of Cu into the TiO_2 matrix upon the HT, i.e., Cu doping.

In addition to Ti, O, Cu and C (adventitious contamination), Na, Ca and Si were detected (Fig. S3, Table S1). These elements originate from the soda-lime glass that was used as a substrate. They were detected as some area of glass substrate was uncovered due to the shrinkage of PS template, and thus became visible in the XPS surface analysis (Fig. S1).

Fig. 2 presents the measured XRD patterns for the plain TiO_2 (no Cu), 150 c Cu and 150 c Cu + HT samples. The XRD patterns verify that the crystalline phase of the prepared TiO_2 IO structure was anatase. All typical peaks of the anatase phase were well defined at 25.6°, 38.2°, 48.6°, 54.2°, 55.4° and 63.0°, which match well to (101), (004), (200), (105), (211) and (204) crystal planes. The peak at around 23° was observed in all samples, which originated from the amorphous sodalime glass substrate used to fabricate the materials [26]. However, neither CuO nor Cu_2O peaks from deposited thin films were detected in the spectra because of a small interaction volume of the deposited film or due to amorphous structure of ALD Cu. The XRD patterns of the heated samples also showed no differences compared to the unheated one. Hence, the XRD pattern confirmed that neither the ALD process nor the HT induced new phases to the anatase IO structure. López et al. reported similar XRD patterns for anatase TiO_2 doped with 0.1–5.0% Cu upon calcination at 500 °C and concluded interstitial incorporation of Cu into the TiO_2 [23]. The same observation also has been reported by Lee et al. where Cu was incorporated into TiO_2 in form of single-atom dopant, no peaks of Cu was observed even at high Cu concentrations [8]. Thus, no conclusive interpretation of Cu within the TiO_2 structure can be made from the XRD patterns.

Optical absorption of the prepared reference TiO_2 IO and Cu coated TiO_2 IO structure was measured by UV–Visible diffuse reflection spectroscopy (Fig. 3). Internal absorption of TiO_2 started approximately from 370 nm reaching a maximum deep in the UV range [27]. A broad photonic band corresponding to the photonic band gap (PBG) of TiO_2 IO structure was found in the range of 375–600 nm. The stop band of IO structure can be tailored by the used template size [28]. ALD deposited Cu did not have a significant effect on the photonic band gap (PBG) of TiO_2 IO even after heating up to 550 °C for 1 h. Only minor redshift (<10 nm) in the bandgap absorption edge was observed for Cu coated samples after the HT. On the other hand, similarly minor effect was reported by López et al. with small (0.1–0.5%) Cu loadings in Cu-doped TiO_2 [23]. Higher (5.0%) Cu-loading was reported to induce absorption in the 400–600 nm range that overlaps with the broad PBG of the IO structure.

3.2. Photocatalytic activity

In general, the photocatalytic reaction takes place when the catalyst is triggered by photons with energy of equivalent or higher energy than the electronic bandgap energy of the semiconductor followed by electron-hole pair generation. These photogenerated electron-hole pairs can diffuse to the surface and react with the absorbed species such as oxygen and water producing highly reactive radicals, which induce the degradation of organic pollutants [29]. Fig. 4 shows the band position and possible redox reaction of ALD Cu coated TiO_2 IO materials. $Cu_2^{+}O$ was the main component in our ALD Cu–TiO_2 IO materials evidenced by XPS results (Fig. 1d) and by previous study [10]. CuO is expected to form

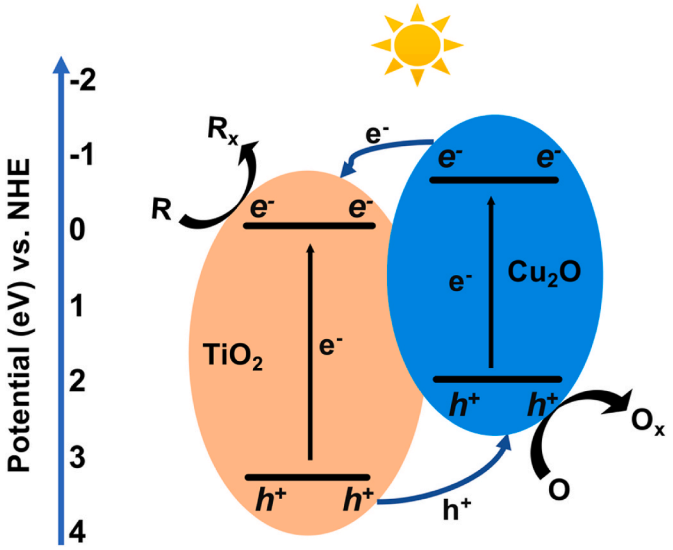

Fig. 4. Schematic illustration the possible redox reaction in ALD Cu coated on TiO_2 IO.

only at the surface when the sample exposed to the air with time. When TiO_2 IO is coated by Cu_2O, a p-n junction is formed between n-type TiO_2 IO and p-type Cu_2O [30,31]. Under illumination, electrons (e^-) and holes (h^+) are formed in the conduction band (CB) and valence band (VB) of Cu_2O and TiO_2 IO. The excited e^- in the CB of Cu_2O will migrate toward the CB of TiO_2 as the CB potential of Cu_2O is more negative than TiO_2 [32]. Likewise, the h^+ generated in the VB of TiO_2 will move toward VB of Cu_2O as VB potential of TiO_2 is more positive than Cu_2O [33]. In this way, the separated e^- in the CB of TiO_2 will take part in the reduction reaction and h^+ in the VB of Cu_2O will participate in the oxidation reaction to keep the charge balance. The formation of p-n junction between two semiconductors results in the efficient charge separation, which in-turn gives higher photocatalytic reaction efficiency [34–36]. It is noteworthy that the photocatalytic performance of the prepared material could also be improved by the presence of Cu metallic due to the localized surface plasmonic resonance effect [37]. However, in this work the presence of Cu metallic is unlikely as Cu is easily oxidized in the ambient condition.

Photodegradation of methylene blue (MB) is a commonly applied test to determine the photocatalytic activity of thin films and surfaces [38]. MB photodegradation on a surface is widely considered to follow the Langmuir–Hinshelwood mechanism in the first order, $c = c_0 \exp(-kt)$, for which the rate constant (k) can be analyzed as the slope of $-\ln(c/c_0)$ vs. time curve (Fig. S4) [39]. Fig. 5a presents the performance of the IO samples in photodecomposition of MB under UVA irradiation. The bare glass was measured as a control sample showing negligible activity. 150 c Cu sample inactivated the photocatalytic activity of TiO_2 IO towards MB photodegradation, whereas 10 c Cu sample slightly reduced the activity of TiO_2 IO. Strong dissolution of Cu in the aqueous MB solution during the test was measured by ICP-MS for ALD Cu sample without the HT (Table S2) that indicates low chemical stability of ALD Cu. Leaching of Cu from the HT samples was significantly smaller, only 5%, compared to the as-deposited ALD Cu samples. Samples after the heat treatment process exhibited an improved photocatalytic activity up to 175% and 150% for 10 c Cu + HT and 150 c Cu + HT, respectively. This improvement can be explained by several factors. First, the heat treatment improved the interface between Cu and TiO_2 followed by enhanced charge separation. Second, the heat treatment reduced Cu^{2+} to Cu^+ in 150 c Cu + HT, which has potential for a higher reactive oxygen species generation rate [40]. Finally, the position of CB and VB in both Cu_2O and TiO_2 were well-suited for redox reactions of MB [41]. The similar system of CuO and Cu deposited on TiO_2 nanobelt reported to have higher activity in the degradation of methyl orange (MO) with 3- and 5-times improvement compared to undeposited samples, respectively [42]. Because of the low chemical stability of ALD Cu in aqueous conditions, photocatalytic tests were also performed in the gas-phase.

Photocatalytic activity of the TiO_2 IO and Cu coated TiO_2 IO samples was measured by the decomposition of C_2H_2 gas under a full source spectrum by High Power Xenon Light Sources. The photocatalytic activity of samples was recorded by monitoring C_2H_2 decomposition to CO_2 at different times as represented in Fig. 5b. The uncoated TiO_2 IO sample showed the highest activity (3 ppm/min), whereas ALD functionalized samples exhibited lower activities with decrease of 58%, 49% for 10 c Cu, 150 c Cu samples compared to no Cu sample, respectively. The HT did not improve the activity above the uncoated TiO_2 indicating that Cu on the surface is not beneficial to the photocatalytic C_2H_2 oxidation activity. It has been reported the photocatalytic activity of TiO_2 depends on the amount of both physisorbed and chemisorbed water molecules on its surface [43]. Therefore, the observed reduction in the activity of the ALD Cu deposited samples can result from the reduction of water molecules, which existed in the technical air, on the sample surface. Since Cu layer is hydrophobic [44], it may act as a barrier layer on the sample surface. This layer can prevent the

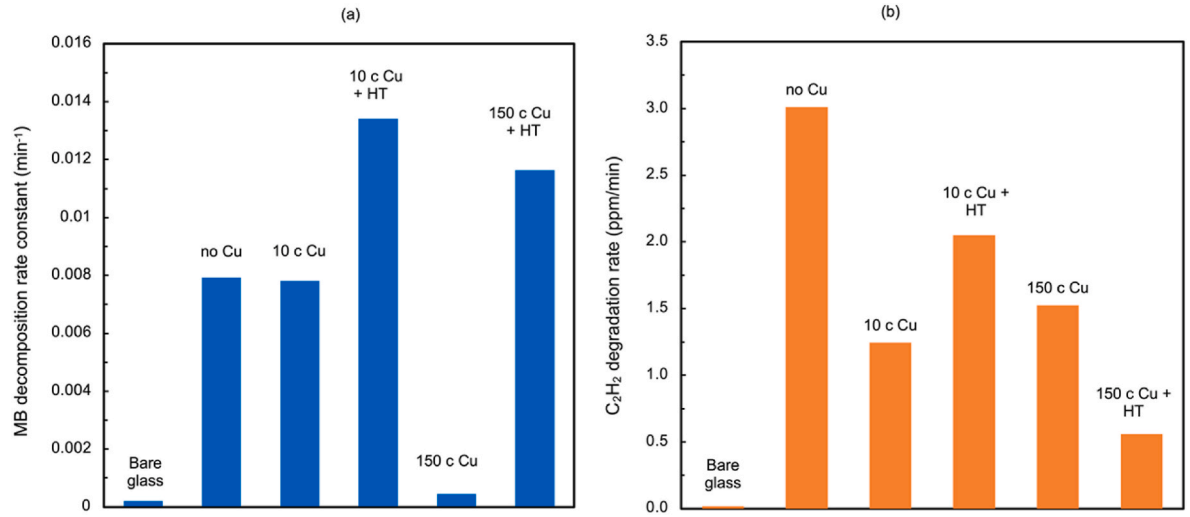

Fig. 5. (a) Photocatalytic degradation of MB under UVA irradiation. Rate constants were analyzed as the slope of –ln(c/c0) vs. time curves, (b) Photodegradation of C_2H_2 under UVA light as a function of CO_2 production.

absorption of physisorbed molecular water and chemisorbed hydroxide species that are needed to form reactive radicals. In the presence of water vapor the CO_2 resulting from the oxidation of C_2H_2 may further react to form CH_4 and other species that would decrease the apparent activity. Indeed, Cu on TiO_2 has been reported to catalyze the CO_2 reduction reaction.

The CO_2 reduction on the photocatalyst surface under the light irradiation is a complex process. First, CO_2 molecules are absorbed on the surface of photocatalyst and are activated for reduction. The absorption also changes the structure of CO_2 from a linear molecule to a bent structure, resulting in a reduction in the level of lowest unoccupied molecular orbital (LUMO). This in turn lowers the barrier for acquiring electrons under irradiation [45]. When incident light is irradiated on the photocatalyst surface, the electrons are generated and then migrated to the absorbed CO_2 to start the reduction reaction. This reaction is thought to proceed through various intermediate free radicals and products [46]. In this study, the photocatalytic activity of samples for CO_2 reduction in the presence of water vapor was studied in the gas-phase under UVA irradiation. The reaction may result in various products but the formation of CH_4 was considered as a proof of the CO_2 reduction activity [24].

Many reaction mechanisms for CO_2 photoreduction on a semiconductor surface have been proposed such as formaldehyde pathway [47], the glyoxal pathway [48] and carbene pathway [49]. From these the carbene pathway is expensively accepted for the formation of CH_4 as the main product [46]. The electron paramagnetic resonance (EPR) and electron spin resonance (ESR) methods has been used to further confirm the carbene pathway mechanism [49,50]. In the carbene pathway, photoexcited electron from photocatalyst is injected to the absorbed CO_2 to form anion radical $CO_2^{\bullet -}$. This electron has a highly negative electrochemical potential of −1.9 V compared to a normal hydrogen electrode (NHE) [50]. Hence, the semiconductors to undergo reduction is quite unlikely. Therefore, it is assumed that right after the formation of $CO_2^{\bullet -}$ radical, it reacts with H^+ (generated from the oxidation of water) and e^- to form intermediate radicals and products. This process is commonly named as "proton-assisted multielectron reduction" (PMR) and is widely tolerable for the photoreduction of CO_2. The main product CH_4 is formed after the radicals and products formed at the intermediate steps further undergo a series of PMRs. Therefore, based on the understanding of the PMR via the carbene pathway, we suggest an overall process for the reduction of CO_2 as displayed eqs 1- 6 below. First, upon receiving the photon from the incident light, the photogenerated charge carriers (e^- and h^+) are produced at the ALD Cu–TiO_2 IO photocatalyst surface (eq (1)). The absorbed H_2O reacts with h^+ to generate protons (H^+) and hydroxyl radicals ($OH^\bullet$) (eq (2)), while the absorbed CO_2 reacts with the electrons (e^-) to form $CO_2^{\bullet -}$ radical (eq (3)). This radical undergoes reduction process forming CO (eq (4)). The formed CO reacts with e^- and H^+ further to form the surface adsorbed C (eq (5)), which then further reacts with electrons and proton to form methane as a major product (eq (6)).

$$Cu\text{–}TiO_2 + hv \rightarrow e^-_{CB} + h^+_{VB} \quad (1)$$

$$H_2O + h^+ \rightarrow H^+ + OH^- \quad (2)$$

$$CO_2 + e^- \rightarrow CO_2^{\bullet -} \quad (3)$$

$$CO_2^{\bullet -} + e^- + H^+ \rightarrow CO + OH^- \quad (4)$$

$$CO + 2e^- + H^+ \rightarrow C + OH^- \text{-} \quad (5)$$

$$C + 4e^- + H^+ \rightarrow CH_4 \quad (6)$$

Fig. 6 shows the CH_4 production rates for the samples. As expected, more CH_4 was formed when increased the thickness of ALD Cu layer. A plain microscopy slide was used as a control sample at the same condition and showed negligible activity. Therefore, it is probable that the formation of CH_4 was due to the photoreduction of CO_2 but not the oxidation of surface-bound organics. The TiO_2 IO itself produced up to

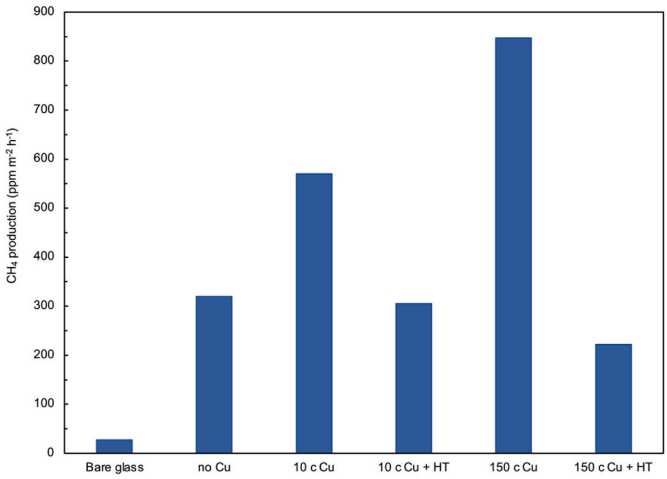

Fig. 6. Photocatalytic CH_4 formation from CO_2 and H_2O in the gas-phase under UVA irradiation.

nearly 350 ppm m^{-2} h^{-1} compared to no CH_4 production of pristine TiO_2 reported by Bhattacharyya et al. [51]. The CH_4 production rate were increased to 183% and 270% for 10 c Cu and 150 c Cu samples compared to reference TiO_2 IO indicating that the ALD Cu process can enhance the surface catalytic activity of TiO_2 IO. The addition of Cu was favored for the formation of CH_4 rather than other product (i.e., H_2 or CO) as observed in other studies [52,53]. The higher selectivity for CH_4 formation after adding Cu layer is mainly attributable to the improved electron traps, and the increased possibility of multi-electron reactions ($CO_2 + 8e^- + 6H^+ \rightarrow CH_4 + 2OH^-$). The experimental results together with XPS data suggest that the addition of either Cu_2O or CuO onto the TiO_2 IO surface can increase CH_4 evolution. When Cu^+ existed in the sample, the CH_4 formation was facilitated by the synergy between Cu^+ species and the surface defect site [54]. Cu^{2+} can be an effective electron traps to reduce the recombination rate as Cu^{2+} ion has an unfilled 3d shell and the reduction of Cu^{2+} is thermodynamically feasible [55]. The electrons generated in Cu can migrate into the CB of TiO_2 and participate in the reduction of adsorbed CO_2 whereas the holes flow in the revert path to conduct the oxidization of the adsorbed H_2O producing H^+ and O_2.

The heat treatment process (550 °C, 1 h) for ALD Cu coated TiO_2 IO samples sharply decreased (>50%) the activity in the CO_2 photoreduction reaction to the level of uncoated TiO_2 IO and below. This contradicts with the MB test result where the HT increased the activity. The presence of the Cu^{2+} state favors the adsorption of CO_2 on the surface of the catalysts while the presence of Cu/Cu^+ states take part in the electrochemical reaction to convert adsorbed CO_2 to hydrocarbons [56,57]. Thus, the oxidation of Cu^+ to Cu^{2+} and decreased amount of Cu^{2+} on the TiO_2 IO surface after the HT may have lowered the adsorption of CO_2 on the photocatalysts and led to decrease in the activity for CO_2 conversion [58].

The stability and regeneration of the photocatalyst were tested using reference TiO_2 IO sample (Figure S5). Without any thermal treatment between the consecutive tests, the CH_4 production rate decreased sharply down to 25% of the initial value. Drying in an oven at 80 °C for 16 h improved the activity by 45% and a heat treatment at 550 °C for 1 h recovered 76% of the initial activity. The decrease in activity may have resulted from two reasons. First, the adsorption of some reaction intermediate species that require heat treatment for desorption and to recover photocatalyst activity [25,17]. Second, the consumption of OH groups and Cu active sites by holes after each cycle were also reduced the activity of the materials [58]. The photocatalyst recovery after the heat treatment at 550 °C was higher than the change in activity of ALD Cu coated samples upon the same heat-treatment. Therefore, we can conclude that while the ALD Cu on IO TiO_2 improved the photocatalytic

CO_2 reduction activity, the heat treatment induced changes in ALD Cu coated samples that resulted in a decreased activity.

The antimicrobial activity was assessed using a bacterial touch test on the functionalized materials. The post-deposition heat treatment samples were chosen for the test due to their improved photocatalytic performance without detachment of the Cu layer into liquid media. The test was conducted on four samples: 10 c Cu + HT, 150 c Cu + HT, no Cu, and a plain microscope glass as a control. The tests were carried out using Gram-positive bacteria (*S. aureus*) under ambient light with 24 h and 48 h exposure time as summarized in Table 2. The number of CFUs were quantitatively calculated from the blood agar plates as shown in the Supplementary information Fig. S. 6. The antimicrobial tests were also performed with Gram-negative bacteria *Escherichia coli* (*E. coli*, ATCC 25922 0,5 McF 50 μl) but no growth was observed on all samples including the bare glass under the test conditions (Table S3). A decrease in the growth of Gram-positive *S. aureus* was observed for the Cu coated samples compared to the reference TiO_2 IO (Fig. S6). A significant decrease in the CFU count of *S. aureus* was observed on TiO_2 IO coated with 10 c Cu + HT sample. This observation is in good agreement with previous finding as the 10 c Cu + HT sample showing the highest photodegradation of pollutants. High antimicrobial activity of ALD Cu coated samples can be attributed to the high generation rate of reactive oxygen species on the sample surface as well as the cytotoxicity of Cu species [59].

4. Conclusions

TiO_2 IO structures were functionalized with sub-monolayer amount of Cu by ALD. The effect of functionalization was tested in terms of photocatalytic activity to decompose MB in the liquid phase, the photodegradation of C_2H_2 and CO_2 reduction in gas phase as well as the antimicrobial activity towards *S. aureus*. Without post-deposition HT at 550 °C the ALD Cu dissolved in aqueous MB solution. The HT induced desorption of loosely bound ALD $Cu^{+/2+}$ from the TiO_2 IO surface and the remaining $Cu^{+/2+}$ was reduced to Cu^{+}. The sub-monolayer amount of Cu did not induce any change in neither optical nor structural properties of TiO_2 IO.

ALD Cu without any post-deposition HT decreased the photo degradation rate of both C_2H_2 and MB but improved the activity towards CO_2 reduction. ALD Cu increased MB photodegradation rate and antimicrobial activity only after HT at 550 °C, which was linked to the improved chemical stability Cu after the HT. The same HT decreased the activity towards CO_2 reduction and decomposition of C_2H_2.

To conclude, our results show that the photocatalytic and antimicrobial activity of TiO_2 IO can be tailored by the addition of a sub-monolayer amounts of Cu with performance depending on the targeted reaction. Most promisingly, the ALD Cu mediated improvement in the MB photodegradation activity has potential application in UV water purification systems where TiO_2 IO can serve as photocatalyst membrane. In general, TiO_2 IO framework showed the superior activity in CO_2 reduction compared to that of pristine TiO_2 reported in other studies. The addition of Cu on the TiO_2 IO framework further improved the performance of the as prepared materials.

CRediT authorship contribution statement

Khai Pham: Conceptualization, Investigation, Writing – original draft, revision. **Harri Ali-Löytty:** Conceptualization, Investigation. **Jesse Saari:** Investigation. **Muhammad Zubair:** Investigation. **Mika Valden:** Supervision, Writing – review & editing. **Kimmo Lahtonen:** Investigation. **Niko Kinnunen:** Investigation. **Marianne Gunell:** Investigation. **Jarkko J. Saarinen:** Conceptualization, Project administration, Supervision, Writing – review & editing.

Declaration of competing interest

The authors declare that they have no known competing financial interests or personal relationships that could have appeared to influence the work reported in this paper.

Acknowledgements

K.P. wishes to thank UEF SCITECO doctoral program for a research position. J.S. was supported by The Vilho, Yrjö and Kalle Väisälä Foundation of the Finnish Academy of Science and Letters. This work was supported by Jane & Aatos Erkko Foundation (Project 'Solar Fuels Synthesis') and by Business Finland (TUTLi project 'Liquid Sun') (Decision Number 1464/31/2019). JJS acknowledges the Academy of Finland funding (339 554). This work is part of the Academy of Finland Flagship Programme, Photonics Research and Innovation (PREIN) (Decision Numbers 320165, 320166).

Appendix A. Supplementary data

Supplementary data to this article can be found online at https://doi.org/10.1016/j.optmat.2022.112695.

References

[1] K. Pham, F. Temerov, J.J. Saarinen, Multicompound inverse opal structures with gold nanoparticles for visible light photocatalytic activity, Mater. Des. 194 (2020), https://doi.org/10.1016/j.matdes.2020.108886.
[2] J. Liu, M. Liu, X. Yang, H. Chen, S.F. Liu, J. Yan, Photo-redeposition synthesis of bimetal Pt–Cu Co-catalysts for TiO2 photocatalytic solar-fuel production, ACS Sustain. Chem. Eng. 8 (2020) 6055–6064, https://doi.org/10.1021/acssuschemeng.0c00969.
[3] K. Pham, S. Pelisset, N. Kinnunen, P. Karvinen, T.K. Hakala, J.J. Saarinen, Controlled photocatalytic activity of TiO2 inverse opal structures with atomic layer deposited (ALD) metal oxide thin films, Mater. Chem. Phys. (2021), 125533, https://doi.org/10.1016/j.matchemphys.2021.125533.
[4] P. Basnet, E. Anderson, Y. Zhao, Hybrid CuxO-TiO2 nanopowders prepared by ball milling for solar energy conversion and visible-light-induced wastewater treatment, ACS Appl. Nano Mater. 2 (2019) 2446–2455, https://doi.org/10.1021/acsanm.9b00325.
[5] S. López-Ayala, M.E. Rincón, Catalytic and photocatalytic performance of mesoporous CuxO–TiO2, J. Photochem. Photobiol. Chem. 222 (2011) 249–257, https://doi.org/10.1016/j.jphotochem.2011.05.026.
[6] D. Barreca, G. Carraro, A. Gasparotto, C. Maccato, O.I. Lebedev, A. Parfenova, S. Turner, E. Tondello, G. van Tendeloo, Tailored vapor-phase growth of CuxO-TiO2 (x = 1, 2) nanomaterials decorated with Au particles, Langmuir 27 (2011) 6409–6417, https://doi.org/10.1021/la200698t.
[7] H. Kim, M.Y. Lee, S.-H. Kim, S.I. Bae, K.Y. Ko, H. Kim, K.-W. Kwon, J.-H. Hwang, D.-J. Lee, Highly-conformal p-type copper(I) oxide (Cu2O) thin films by atomic layer deposition using a fluorine-free amino-alkoxide precursor, Appl. Surf. Sci. 349 (2015) 673–682, https://doi.org/10.1016/j.apsusc.2015.05.062.
[8] B.-H. Lee, E. Gong, M. Kim, S. Park, H.R. Kim, J. Lee, E. Jung, C.W. Lee, J. Bok, Y. Jung, Y.S. Kim, K.-S. Lee, S.-P. Cho, J.-W. Jung, C.-H. Cho, S. Lebègue, K.T. Nam, H. Kim, S.-I. In, T. Hyeon, Electronic interaction between transition metal single-atoms and anatase TiO2 boosts CO2 photoreduction with H2O, Energy Environ. Sci. 15 (2022) 601–609, https://doi.org/10.1039/D1EE01574E.
[9] E. Gong, S. Ali, C.B. Hiragond, H.S. Kim, N.S. Powar, D. Kim, H. Kim, S.-I. In, Solar fuels: research and development strategies to accelerate photocatalytic CO2 conversion into hydrocarbon fuels, Energy Environ. Sci. 15 (2022) 880–937, https://doi.org/10.1039/D1EE02714J.
[10] J.R. Avila, C.R. Eddy, V.D. Wheeler, Comprehensive characterization of copper oxide atomic layer deposition using water or ozone with enhanced bis-(dimethylamino-2-propoxide) copper delivery, J. Vac. Sci. Technol. 38 (2020), 042403, https://doi.org/10.1116/6.0000248.
[11] N. Fairley, CasaXPS: Spectrum Processing Software for XPS, AES and SIMS, (n.d.).
[12] J.H. Scofield, Hartree-Slater subshell photoionization cross-sections at 1254 and 1487 eV, J. Electron. Spectrosc. Relat. Phenom. 8 (1976) 129–137, https://doi.org/10.1016/0368-2048(76)80015-1.
[13] S. Tanuma, C.J. Powell, D.R. Penn, Calculations of Electron Inelastic Mean Free Paths. V. Data for 14 Organic Compounds over the 50-2000 eV Range, 1993.
[14] J. Saari, H. Ali-Löytty, M. Honkanen, A. Tukiainen, K. Lahtonen, M. Valden, Interface engineering of TiO2 photoelectrode coatings grown by atomic layer deposition on silicon, ACS Omega 6 (2021) 27501–27509, https://doi.org/10.1021/acsomega.1c04478.
[15] R. Khan, H. Ali-Löytty, A. Tukiainen, N. v Tkachenko, Comparison of the heat-treatment effect on carrier dynamics in TiO2 thin films deposited by different methods, Phys. Chem. Chem. Phys. 23 (2021) 17672–17682, https://doi.org/10.1039/D1CP02716F.

[16] M. Gunell, J. Haapanen, K.J. Brobbey, J.J. Saarinen, M. Toivakka, J.M. Mäkelä, P. Huovinen, E. Eerola, Antimicrobial characterization of silver nanoparticle-coated surfaces by "touch test" method, Nanotechnol. Sci. Appl. 10 (2017) 137–145, https://doi.org/10.2147/NSA.S139505.

[17] B. Lafuente, R.T. Downs, H. Yang, N. Stone, in: T. Armbruster, R.M. Danisi (Eds.), 1. The Power of Databases: the RRUFF Project, De Gruyter (O), 2015, pp. 1–30, https://doi.org/10.1515/9783110417104-003.

[18] S. Zhang, X. Gong, Q. Shi, G. Ping, H. Xu, A. Waleed, G. Li, CuO nanoparticle-decorated TiO2-nanotube heterojunctions for direct synthesis of methyl formate via photo-oxidation of methanol, ACS Omega 5 (2020) 15942–15948, https://doi.org/10.1021/acsomega.0c01169.

[19] M.C. Biesinger, Advanced analysis of copper X-ray photoelectron spectra, Surf. Interface Anal. 49 (2017) 1325–1334, https://doi.org/10.1002/sia.6239.

[20] U. Diebold, The surface science of titanium dioxide, Surf. Sci. Rep. 48 (2003) 53–229, https://doi.org/10.1016/S0167-5729(02)00100-0.

[21] K. Mimura, J.-W. Lim, M. Isshiki, Y. Zhu, Q. Jiang, Brief review of oxidation kinetics of copper at 350 °C to 1050 °C, Metall. Mater. Trans. 37 (2006) 1231–1237, https://doi.org/10.1007/s11661-006-1074-y.

[22] J. Choi, H. Park, M.R. Hoffmann, Effects of single metal-ion doping on the visible-light photoreactivity of TiO2, J. Phys. Chem. C 114 (2010) 783–792, https://doi.org/10.1021/jp908088x.

[23] R. López, R. Gómez, M.E. Llanos, Photophysical and photocatalytic properties of nanosized copper-doped titania sol–gel catalysts, Catal. Today 148 (2009) 103–108, https://doi.org/10.1016/j.cattod.2009.04.001.

[24] G. Colón, M. Maicu, M.C. Hidalgo, J.A. Navío, Cu-doped TiO2 systems with improved photocatalytic activity, Appl. Catal. B Environ. 67 (2006) 41–51, https://doi.org/10.1016/j.apcatb.2006.03.019.

[25] U. Diebold, J.-M. Pan, T.E. Madey, Growth mode of ultrathin copper overlayers on ${\mathrm{TiO}}_{2}$(110), Phys. Rev. B 47 (1993) 3868–3876, https://doi.org/10.1103/PhysRevB.47.3868.

[26] A. Bernasconi, M. Dapiaggi, C. Milanese, M. Alloni, A. Pavese, Structure of soda-lime-aluminosilicate glasses as revealed by in-situ synchrotron powder diffraction experiments, J. Non-Cryst. Solids 568 (2021), 120932, https://doi.org/10.1016/j.jnoncrysol.2021.120932.

[27] F. Temerov, K. Pham, P. Juuti, J.M. Mäkelä, E.V. Grachova, S. Kumar, S. Eslava, J. J. Saarinen, Silver-Decorated TiO_2Inverse opal structure for visible light-induced photocatalytic degradation of organic pollutants and hydrogen evolution, ACS Appl. Mater. Interfaces 12 (2020), https://doi.org/10.1021/acsami.0c08624.

[28] R.C. Schroden, M. Al-Daous, C.F. Blanford, A. Stein, Optical properties of inverse opal photonic crystals, Chem. Mater. 14 (2002) 3305–3315, https://doi.org/10.1021/cm020100z.

[29] R. Saravanan, F. Gracia, A. Stephen, Basic principles, mechanism, and challenges of photocatalysis. https://doi.org/10.1007/978-3-319-62446-4_2, 2017, 19-40.

[30] M. Muscetta, R. Andreozzi, L. Clarizia, I. di Somma, R. Marotta, Hydrogen production through photoreforming processes over Cu2O/TiO2 composite materials: a mini-review, Int. J. Hydrogen Energy 45 (2020) 28531–28552, https://doi.org/10.1016/j.ijhydene.2020.07.225.

[31] Y. Cheng, X. Gao, X. Zhang, J. Su, G. Wang, L. Wang, Synthesis of a TiO2–Cu2O composite catalyst with enhanced visible light photocatalytic activity for gas-phase toluene, New J. Chem. 42 (2018) 9252–9259, https://doi.org/10.1039/C8NJ00409A.

[32] Y. Bessekhouad, D. Robert, J.-V. Weber, Photocatalytic activity of Cu2O/TiO2, Bi2O3/TiO2 and ZnMn2O4/TiO2 heterojunctions, Catal. Today 101 (2005) 315–321, https://doi.org/10.1016/j.cattod.2005.03.038.

[33] J. Wang, G. Ji, Y. Liu, M.A. Gondal, X. Chang, Cu2O/TiO2 heterostructure nanotube arrays prepared by an electrodeposition method exhibiting enhanced photocatalytic activity for CO2 reduction to methanol, Catal. Commun. 46 (2014) 17–21, https://doi.org/10.1016/j.catcom.2013.11.011.

[34] L. Huang, F. Peng, H. Wang, H. Yu, Z. Li, Preparation and characterization of Cu2O/TiO2 nano–nano heterostructure photocatalysts, Catal. Commun. 10 (2009) 1839–1843, https://doi.org/10.1016/j.catcom.2009.06.011.

[35] L. Yang, S. Luo, Y. Li, Y. Xiao, Q. Kang, Q. Cai, High efficient photocatalytic degradation of p-nitrophenol on a unique Cu2O/TiO2 p-n heterojunction network catalyst, Environ. Sci. Technol. 44 (2010) 7641–7646, https://doi.org/10.1021/es101711k.

[36] G. Li, J. Huang, J. Chen, Z. Deng, Q. Huang, Z. Liu, W. Guo, R. Cao, Highly active photocatalyst of Cu2O/TiO2 octahedron for hydrogen generation, ACS Omega 4 (2019) 3392–3397, https://doi.org/10.1021/acsomega.8b03404.

[37] M. Sayed, J. Yu, G. Liu, M. Jaroniec, Non-noble plasmonic metal-based photocatalysts, Chem. Rev. 122 (2022) 10484–10537, https://doi.org/10.1021/acs.chemrev.1c00473.

[38] International Organization for Standardization, Fine ceramics (advanced ceramics, advanced technical ceramics) — determination of photocatalytic activity of surfaces in an aqueous medium by degradation of methylene blue, ISO 10678: 2010, Retrieved from, https://www.iso.org/standard/46019.html, 2010. (Accessed 9 December 2021).

[39] A. Houas, H. Lachheb, M. Ksibi, E. Elaloui, C. Guillard, J.-M. Herrmann, Photocatalytic degradation pathway of methylene blue in water, Appl. Catal. B Environ. 31 (2001) 145–157, https://doi.org/10.1016/S0926-3373(00)00276-9.

[40] P. Basnet, Y. Zhao, Tuning the CuxO nanorod composition for efficient visible light induced photocatalysis, Catal. Sci. Technol. 6 (2016) 2228–2238, https://doi.org/10.1039/c5cy01464f.

[41] Y. He, P. Basnet, S.E.H. Murph, Y. Zhao, Ag nanoparticle embedded TiO2 composite nanorod arrays fabricated by oblique angle deposition: toward plasmonic photocatalysis, ACS Appl. Mater. Interfaces 5 (2013) 11818–11827, https://doi.org/10.1021/am4035015.

[42] M. Logar, I. Bračko, A. Potočnik, B. Jančar, Cu and CuO/titanate nanobelt based network assemblies for enhanced visible light photocatalysis, Langmuir 30 (2014) 4852–4862, https://doi.org/10.1021/la5008704.

[43] K. Shirai, G. Fazio, T. Sugimoto, D. Selli, L. Ferraro, K. Watanabe, M. Haruta, B. Ohtani, H. Kurata, C. di Valentin, Y. Matsumoto, Water-assisted hole trapping at the highly curved surface of nano-TiO2 photocatalyst, J. Am. Chem. Soc. 140 (2018) 1415–1422, https://doi.org/10.1021/jacs.7b11061.

[44] S.L. Shinde, K.K. Nanda, Facile synthesis of large area porous Cu2O as super hydrophobic yellow-red phosphors, RSC Adv. 2 (2012) 3647–3650, https://doi.org/10.1039/C2RA20066J.

[45] V.P. Indrakanti, J.D. Kubicki, H.H. Schobert, Photoinduced activation of CO2 on Ti-based heterogeneous catalysts: current state, chemical physics-based insights and outlook, Energy Environ. Sci. 2 (2009) 745–758, https://doi.org/10.1039/B822176F.

[46] S.N. Habisreutinger, L. Schmidt-Mende, J.K. Stolarczyk, Photocatalytic reduction of CO2 on TiO2 and other semiconductors, Angew. Chem. Int. Ed. 52 (2013) 7372–7408, https://doi.org/10.1002/anie.201207199.

[47] L.O. Kamila Kočí, Olga Šolcová, Kinetic study of photocatalytic reduction of CO2 over TiO2, Chem. Process Eng. 31 (2010) 375–407.

[48] I.A. Shkrob, N.M. Dimitrijevic, T.W. Marin, H. He, P. Zapol, Heteroatom-transfer coupled photoreduction and carbon dioxide fixation on metal oxides, J. Phys. Chem. C 116 (2012) 9461–9471, https://doi.org/10.1021/jp300123z.

[49] M. Anpo, H. Yamashita, Y. Ichihashi, S. Ehara, Photocatalytic reduction of CO2 with H2O on various titanium oxide catalysts, J. Electroanal. Chem. 396 (1995) 21–26, https://doi.org/10.1016/0022-0728(95)04141-A.

[50] W.H. Koppenol, J.D. Rush, Reduction potential of the carbon dioxide/carbon dioxide radical anion: a comparison with other C1 radicals, J. Phys. Chem. 91 (1987) 4429–4430, https://doi.org/10.1021/j100300a045.

[51] K. Bhattacharyya, G.P. Mane, V. Rane, A.K. Tripathi, A.K. Tyagi, Selective CO2 photoreduction with Cu-doped TiO2 photocatalyst: delineating the crucial role of Cu-oxidation state and oxygen vacancies, J. Phys. Chem. C 125 (2021) 1793–1810, https://doi.org/10.1021/acs.jpcc.0c08441.

[52] B. Fang, Y. Xing, A. Bonakdarpour, S. Zhang, D.P. Wilkinson, Photodriven reduction of CO2 to CH4, ACS Sustain. Chem. Eng. 3 (2015) 2381–2388, https://doi.org/10.1021/acssuschemeng.5b00724.

[53] Y. Li, W.-N. Wang, Z. Zhan, M.-H. Woo, C.-Y. Wu, P. Biswas, Photocatalytic reduction of CO2 with H2O on mesoporous silica supported Cu/TiO2 catalysts, Appl. Catal. B Environ. 100 (2010) 386–392, https://doi.org/10.1016/j.apcatb.2010.08.015.

[54] L. Liu, F. Gao, H. Zhao, Y. Li, Tailoring Cu valence and oxygen vacancy in Cu/TiO2 catalysts for enhanced CO2 photoreduction efficiency, Appl. Catal. B Environ. 134–135 (2013) 349–358, https://doi.org/10.1016/j.apcatb.2013.01.040.

[55] Slamet, H.W. Nasution, E. Purnama, S. Kosela, J. Gunlazuardi, Photocatalytic reduction of CO2 on copper-doped Titania catalysts prepared by improved-impregnation method, Catal. Commun. 6 (2005) 313–319, https://doi.org/10.1016/j.catcom.2005.01.011.

[56] S. Ali, A. Razzaq, H. Kim, S.-I. In, Activity, selectivity, and stability of earth-abundant CuO/Cu2O/Cu0-based photocatalysts toward CO2 reduction, Chem. Eng. J. 429 (2022), 131579, https://doi.org/10.1016/j.cej.2021.131579.

[57] Y.A. Wu, I. McNulty, C. Liu, K.C. Lau, Q. Liu, A.P. Paulikas, C.-J. Sun, Z. Cai, J. R. Guest, Y. Ren, V. Stamenkovic, L.A. Curtiss, Y. Liu, T. Rajh, Facet-dependent active sites of a single Cu2O particle photocatalyst for CO2 reduction to methanol, Nat. Energy 4 (2019) 957–968, https://doi.org/10.1038/s41560-019-0490-3.

[58] L. Liu, C. Zhao, J.T. Miller, Y. Li, Mechanistic study of CO2 photoreduction with H2O on Cu/TiO2 nanocomposites by in situ X-ray absorption and infrared spectroscopies, J. Phys. Chem. C 121 (2017) 490–499, https://doi.org/10.1021/acs.jpcc.6b10835.

[59] A.M. Alotaibi, B.A.D. Williamson, S. Sathasivam, A. Kafizas, M. Alqahtani, C. Sotelo-Vazquez, J. Buckeridge, J. Wu, S.P. Nair, D.O. Scanlon, I.P. Parkin, Enhanced photocatalytic and antibacterial ability of Cu-doped anatase TiO2 thin films: theory and experiment, ACS Appl. Mater. Interfaces 12 (2020) 15348–15361, https://doi.org/10.1021/acsami.9b22056.